Journal of Materiomics 11 (2025) 100858

Contents lists available at ScienceDirect

Journal of Materiomics

journal homepage: www.journals.elsevier.com/journal-of-materiomics/

Research paper

Nonlinear optical response of thermally stable perovskite for near-infrared optical modulator

Jiang Wang [a, ***], Liang Xie [a], Jingjing Liu [b, c], Yuxuan Sun [a], Jinglong Xu [a], Jiacheng Li [d], Zhongying Zhang [e], Chengbing Qin [b, c], Liantuan Xiao [b, c], Guofeng Zhang [b, c], Yonggang Wang [d], Zhichun Yang [b, c, *], Guanghua Cheng [a, **]

[a] School of Artificial Intelligence, Optics and Electronics (iOPEN), Northwestern Polytechnical University, Xi'an, 710072, China
[b] State Key Laboratory of Quantum Optics and Quantum Optics Devices, Institute of Laser Spectroscopy, Shanxi University, Taiyuan, 030006, China
[c] Collaborative Innovation Center of Extreme Optics, Shanxi University, Taiyuan, 030006, China
[d] School of Physics and Information Technology, Shaanxi Normal University, Xi'an, 710119, China
[e] School of Microelectronics, Northwestern Polytechnical University, Xi'an, 710072, China

ARTICLE INFO

Article history:
Received 30 December 2023
Received in revised form
14 February 2024
Accepted 11 March 2024
Available online 6 April 2024

Keywords:
Nonlinear optical
Perovskite
Laser
Optical modulator

ABSTRACT

Metal halide perovskite has generated significant attention due to its high optical absorption coefficient, the tunability of bandgap, and its solution processing properties, all of which have led to a range of applications including solar cells, photodetectors, light-emitting diodes and lasers. However, the material's application as an optical modulator for high-energy ultrafast lasers is still limited by its slow nonlinear optical response, low damage threshold and the inferior stability. Herein, we developed a saturable absorber (SA) with the thermally stable $Cs_{0.15}FA_{0.85}PbI_{2.85}Br_{0.15}$ perovskite thin films as an optical modulator towards the near-infrared nanosecond passively Q-switched Nd:YAG laser generation for the first time. The $Cs_{0.15}FA_{0.85}PbI_{2.85}Br_{0.15}$ perovskite SA optical modulator produced an exceptional nonlinear optical response with a notable modulation depth of 15.1%, an ultrashort recovery time of 52.46 ps, and a high optical damage threshold exceeding 275.9 mJ/cm^2. Of further significance, it displayed an excellent operational stability, and when incorporated into the oscillator of the Nd:YAG laser, allowed for a stable operation of 166 ns pulse laser with a center wavelength of 1.06 μm. The findings provide a pathway for the employment of the $Cs_{0.15}FA_{0.85}PbI_{2.85}Br_{0.15}$ perovskite SA optical modulator in near-infrared ultrafast laser applications.

1. Introduction

The last decades have witnessed the skyrocketed development of metal halide perovskite semiconductors thanks to their remarkable optoelectronic properties [1,2]. Impressively, it brings tremendous potential opportunities since the discovery of nonlinear optical (NLO) response of perovskite semiconductors in 2016 [3]. Particularly, it is being investigated in depth used an saturable absorber (SA) optical modulator for pulse lasers with efficient responses across fast timescale and outstretched laser wavelength ranges [4–7]. Recently, some well-studied perovskite materials have been reported to achieve ultrafast pulsed lasers as SA based on their nonlinear properties, such as excellent saturation light intensity, modulation depth, and nonlinear loss [8–13]. However, its practical application for the efficient photonic devices is still impeded due to the inferior NLO responses and thermal stability of perovskites.

The SA optical modulator is an optical element that operates on the basis of nonlinear saturation absorption characteristics [14]. For efficient short pulse laser, a SA optical modulator with a high optical damage threshold, short recovery time and high stability is in high demand [15–17]. However, the instability of perovskite halides in humid environments, exposure to air, heat, and radiation has hindered their widespread commercial and scientific applications [18]. Particularly, a kind of methylammonium (MA)-free

* Corresponding author.
** Corresponding author.
*** Corresponding author.
E-mail addresses: wjiang@nwpu.edu.cn (J. Wang), yangzhichun@sxu.edu.cn (Z. Yang), guanghuacheng@nwpu.edu.cn (G. Cheng).
Peer review under responsibility of The Chinese Ceramic Society.

https://doi.org/10.1016/j.jmat.2024.03.004

perovskite materials with composition of $Cs_{0.15}FA_{0.85}PbI_{2.85}Br_{0.15}$ exhibits outstanding optoelectronic properties, including lower trap densities, high thermal and phase stability [19–22]. Nevertheless, its exploitation in photonics devices is still limited by the lack of research.

This report describes the first successful demonstration of an effective SA optical modulator with the thermally stable $Cs_{0.15}FA_{0.85}PbI_{2.85}Br_{0.15}$ perovskite for near-infrared lasers. To investigate the NLO properties, we carried out systematical Z-scan measurements, achieving a considerable modulation depth of 15.1%. In particular, the carrier dynamics of $Cs_{0.15}FA_{0.85}PbI_{2.85}Br_{0.15}$ perovskite SA optical modulator was measured by ultrafast pump-probe measurements with an average recovery time of 52.46 ps. Encouragingly, its exhibit an excellent operational stability and a high optical damage threshold over 275.9 mJ/cm^2. Furthermore, an average output power of 338 mW near-infrared nanosecond laser was achieved by integrating $Cs_{0.15}FA_{0.85}PbI_{2.85}Br_{0.15}$ perovskite films SA optical modulator. These findings clearly demonstrate that the $Cs_{0.15}FA_{0.85}PbI_{2.85}Br_{0.15}$ perovskite films showcases exceptional potential as a versatile and highly promising nonlinear optical material that can be effectively used in photonic devices.

2. Experimental section

2.1. Materials

Formamidinium iodide ($CH(NH_2)_2I$, FAI)), lead iodide (PbI_2, >98%), and Cesium bromide (CsBr, 99.99%) were procured from Tokyo Chemical Industry Co. Ltd. N, N-dimethylformamide (DMF, anhydrous, 99.8%), chlorobenzene (anhydrous, 99.8%), and dimethyl sulfoxide (DMSO, anhydrous, ≥99.9%) were purchased from Sigma-Aldrich. Ethanol (analytically pure) and isopropanol were sourced from Sinopharm Chemical Reagent Company in China.

2.2. The preparation of $Cs_{0.15}FA_{0.85}PbI_{2.85}Br_{0.15}$ perovskite films

To deposit the high-quality $Cs_{0.15}FA_{0.85}PbI_{2.85}Br_{0.15}$ perovskite thin films, all the quartz plate substrates were firstly ultrasonically cleaned with the ethanol and isopropanol for 15 min, respectively. Then, substrates were treated by the ultraviolet ozone for 20 min and transferred into the glovebox. The $Cs_{0.15}FA_{0.85}PbI_{2.85}Br_{0.15}$ perovskite thin films were prepared by the traditional one-step spin-coating process, as shown in Fig. 1a. Typically, the $Cs_{0.15}FA_{0.85}PbI_{2.85}Br_{0.15}$ perovskite precursor ink was spread onto the cleaned substrate by a spin coating process at 6,000 r/min for 30 s to form a precursor films. An antisolvent extraction process was carried out during the spin coating process at 12 s using 150 μL of chlorobenzene to form a stable intermediate films, which was then thermally annealed at 150 °C for 20 min to achieve a fully crystallized perovskite thin films used for the SA optical modulator. With regards to the preparation of perovskite precursor ink, 345.8 mg PbI_2, 109.7 mg FAI and 23.9 mg CsBr were introduced to 1 mL mixed DMF:DMSO solvent (volume ratio of 1:4), and stirred overnight.

2.3. Characteristics

2.3.1. Materials characteristics

In this work, the crystal structure of the $Cs_{0.15}FA_{0.85}PbI_{2.85}Br_{0.15}$ perovskite films was determined by X-ray diffraction patterns. The thickness and surface roughness of the $Cs_{0.15}FA_{0.85}PbI_{2.85}Br_{0.15}$ perovskite films were characterized using an Atomic Force Microscope (AFM). The structure and the Electronic Differential System (EDS) spectrum of the $Cs_{0.15}FA_{0.85}PbI_{2.85}Br_{0.15}$ perovskite films were studied using a Scanning Electron Microscope (SEM). The thermal stability of $Cs_{0.15}FA_{0.85}PbI_{2.85}Br_{0.15}$ perovskite samples was measured by a simultaneous thermal analyzer with a heating rate of 10 °C/min from room temperature to 500 °C in Air atmosphere.

2.3.2. Nonlinear optical characteristics of $Cs_{0.15}FA_{0.85}PbI_{2.85}Br_{0.15}$ perovskite films

The nonlinear absorption characteristics of the $Cs_{0.15}FA_{0.85}PbI_{2.85}Br_{0.15}$ perovskite thin films SA were employed by *Z*-scan techniques. *Z*-scan setup was employed in conjunction with an ultrafast laser system featuring a pulse duration of 1.2 ps and a repetition frequency of 100 kHz at 1,030 nm, as shown in Fig. 1b. The ultrafast laser pulses were split into two identical beams. One laser beam passed through the $Cs_{0.15}FA_{0.85}PbI_{2.85}Br_{0.15}$ perovskite thin films, while the other served as a reference beam. The power ratio of two beams reflected $Cs_{0.15}FA_{0.85}PbI_{2.85}Br_{0.15}$ nonlinear optical properties of perovskite thin films. During the measurement process, the translation of the stage allowed the sample to move in and out of the focal region (the waist beam radius of 19.4 μm), causing changes in irradiance and consequently changes in transmittance, thereby yielding the nonlinear absorption coefficient of the $Cs_{0.15}FA_{0.85}PbI_{2.85}Br_{0.15}$ perovskite thin films.

2.4. Laser cavity

In this work, the laser configuration with $Cs_{0.15}FA_{0.85}PbI_{2.85}Br_{0.15}$ perovskite SA optical modulator was in Fig. 1c and a commercial 808 nm quasi-continuous wave diode laser (LD) was used as the pump source in the system. For the gain medium, a Nd^{3+} doped 1.2% Nd:YAG crystal was chosen. The incident light oscillator mirror (with a high transmission film of 808 nm and a high reflectivity film of 1,064 nm (HR), respectively) is integrated at one end of the gain crystal, which effectively reduces the length of the laser oscillator (only 20 mm), allowing the generation of a short pulse laser. The other end is an output coupler (OC curvature of 100 mm) with a 10% transmission at 1,064 nm.

3. Results and discussion

3.1. Material characterizations

To investigate the surface quality of the prepared perovskite films, scanning electron microscopy (SEM) was carried out and the result is presented in Fig. 2a. The optical image of $Cs_{0.15}FA_{0.85}PbI_{2.85}Br_{0.15}$ perovskite films on quartz plate substrate is depicted in the inset of Fig. 2a. Furthermore, the grain size distribution is approximately in a range of 60–150 nm. They clearly illustrate the homogeneous and densely-grained morphology of the prepared $Cs_{0.15}FA_{0.85}PbI_{2.85}Br_{0.15}$ perovskite thin films, which is entirely composed of a well-crystallized and clean surface of $Cs_{0.15}FA_{0.85}PbI_{2.85}Br_{0.15}$ perovskite films without any pinholes. The EDS spectrum displayed in Fig. 2b confirms the presence of I, Pb, Br, and Cs in the perovskite films, and its atom ratio can be matched well to the chemical composition. As shown in Fig. 2c, XRD analysis confirmed that the $Cs_{0.15}FA_{0.85}PbI_{2.85}Br_{0.15}$ perovskite films is highly crystallized. The main XRD diffraction peaks of $Cs_{0.15}FA_{0.85}PbI_{2.85}Br_{0.15}$ are detected at 14.08°, 19.93°, 24.51°, 28.31° and 31.72°, corresponding to the (100), (011), (111), (200) and (012) lattice planes of perovskite, respectively. The diffraction peaks are closely in accordance with the previously reported results [19,23].

The thickness and surface roughness of $Cs_{0.15}FA_{0.85}PbI_{2.85}Br_{0.15}$ perovskite thin films are significant characteristic for measuring the films quality, and they can be characterized by Atomic Force Microscope (AFM). The three-dimensional (3D) AFM morphology image of the $Cs_{0.15}FA_{0.85}PbI_{2.85}Br_{0.15}$ perovskite sample is illustrated

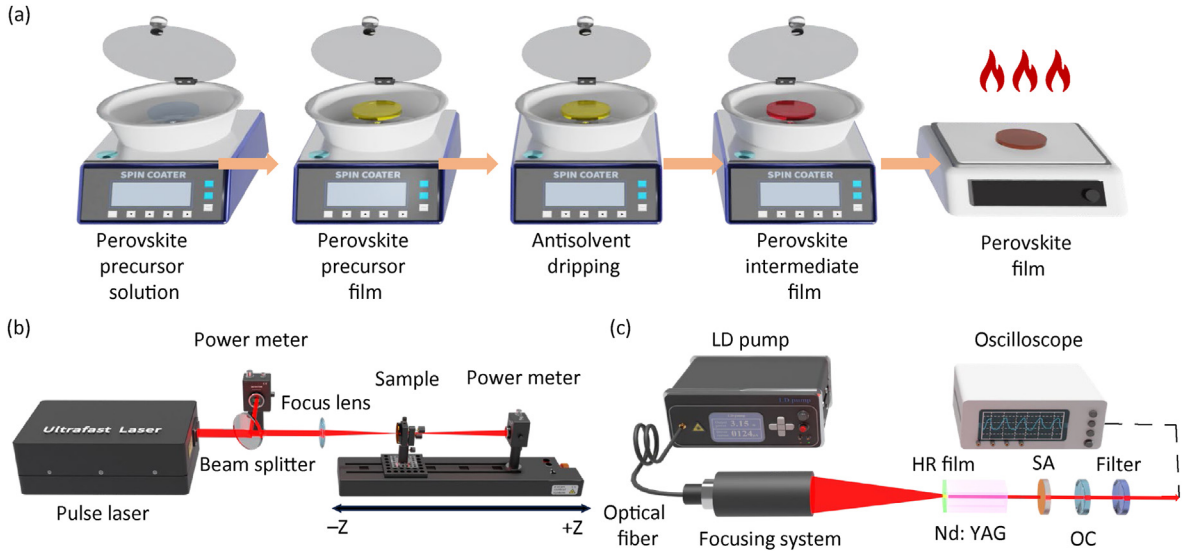

Fig. 1. (a) $Cs_{0.15}FA_{0.85}PbI_{2.85}Br_{0.15}$ perovskite films were prepared; (b) Schematic of *Z*-scan twin-detector technique setups; (c) Laser configuration with $Cs_{0.15}FA_{0.85}PbI_{2.85}Br_{0.15}$ perovskite as the optical modulator.

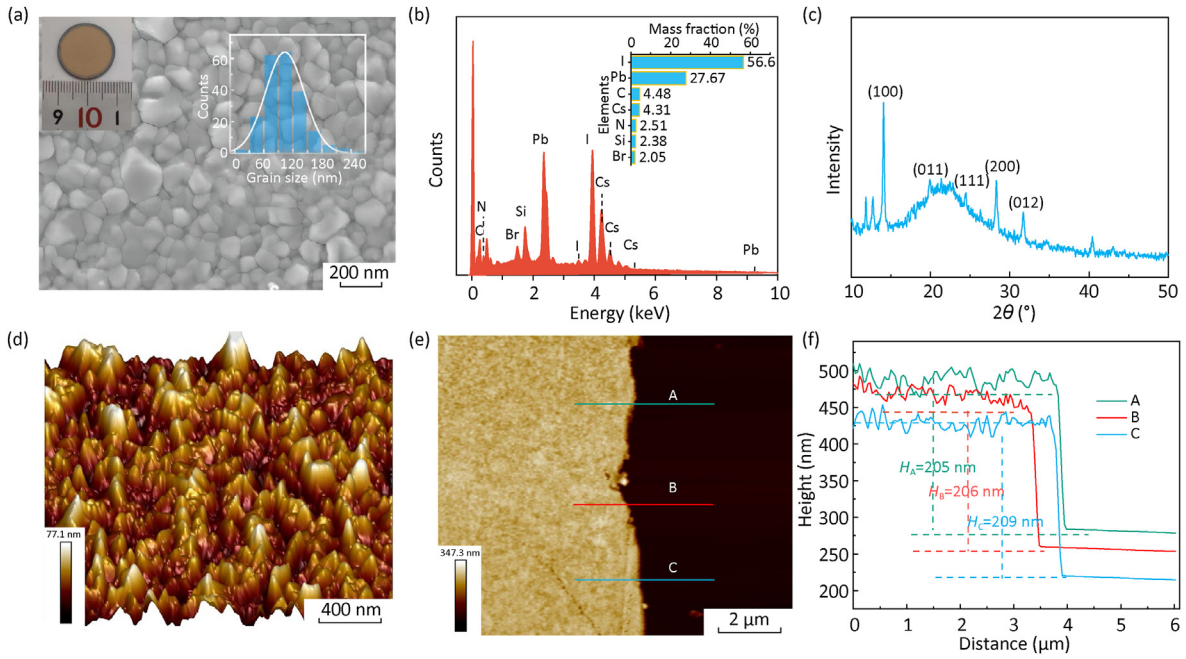

Fig. 2. Characterization of the $Cs_{0.15}FA_{0.85}PbI_{2.85}Br_{0.15}$ perovskite films: (a) SEM image. Inset: the optical image of spin-coated perovskite SA on quartz plate substrate; (b) EDS image; (c) XRD pattern; (d) 3D AFM image; (e) AFM image and (f) cross-sectional height profile of the $Cs_{0.15}FA_{0.85}PbI_{2.85}Br_{0.15}$ perovskite thin films.

in Fig. 2d. The surface roughness of these samples is measured to be 10.6 nm. The AFM image is consistent with the SEM result, both of them indicate that the $Cs_{0.15}FA_{0.85}PbI_{2.85}Br_{0.15}$ perovskite films is highly uniform and without any pinholes, which is conducive to reducing the surface defects and improving its damage resistance as a SA optical modulator device [24]. Utilizing the AFM profiles presented in Fig. 2e and f, three distinct sections were selected for measurements, revealing that the thickness (205, 206, 209 nm) of the perovskite films falls within the range of 205–209 nm. These results indicate that the prepared $Cs_{0.15}FA_{0.85}PbI_{2.85}Br_{0.15}$ perovskite thin films have uniform thickness and smooth surface, which is suitable for the as application in optical devices.

3.2. Damage threshold of the $Cs_{0.15}FA_{0.85}PbI_{2.85}Br_{0.15}$ perovskite films

The laser-induced damage threshold is a crucial parameter for assessing the performance of SA optical modulators. The damage to the $Cs_{0.15}FA_{0.85}PbI_{2.85}Br_{0.15}$ perovskite films can significantly impact its NLO properties under high-energy laser irradiation [25]. To evaluate the laser damage resistance of $Cs_{0.15}FA_{0.85}PbI_{2.85}Br_{0.15}$ perovskite materials, a dedicated testing system was established. This system primarily consists of a laser source and a translation stage. The laser was focused onto the $Cs_{0.15}FA_{0.85}PbI_{2.85}Br_{0.15}$ perovskite films SA using a focusing lens, resulting in a spot radius of approximately 13.4 μm. The damage threshold of the

$Cs_{0.15}FA_{0.85}PbI_{2.85}Br_{0.15}$ perovskite film surface was determined by gradually decreasing the laser energy density. By controlling the laser energy density, different locations on the surface were exposed to varying fluences, resulting in induced damage. As the laser energy density was decreased incrementally, the probability of damage occurrence was monitored. When the laser energy density reached a certain level where the probability of damage occurrence was zero, it was determined as the damage threshold for the $Cs_{0.15}FA_{0.85}PbI_{2.85}Br_{0.15}$ perovskite film.

The traces of the damaged areas were obtained using SEM, as shown in Fig. 3a. At different energy densities, three different locations for damage points were selected, as illustrated in Fig. 3b to d. As the energy density decreased, the extent of damage on the SA reduced, and the corresponding damage probability is shown in Fig. 3e. Consequently, under the given laser parameters, the damage threshold of the $Cs_{0.15}FA_{0.85}PbI_{2.85}Br_{0.15}$ perovskite films SA is between 0.2759 J/cm^2 and 0.2931 J/cm^2. The laser damage testing has demonstrated that the $Cs_{0.15}FA_{0.85}PbI_{2.85}Br_{0.15}$ perovskite thin films SA exhibit remarkable damage resistance.

3.3. Nonlinear optical response of $Cs_{0.15}FA_{0.85}PbI_{2.85}Br_{0.15}$ perovskite films SA

Ultra-rapid carrier dynamics play a key role in the optoelectronic applications of $Cs_{0.15}FA_{0.85}PbI_{2.85}Br_{0.15}$ perovskite films SA optical modulators. The exceptionally quick saturation recovery time of the SA is the key factor enabling the achievement of ultrafast lasers [26,27]. In Fig. 4a, we plotted the transient reflectance spectroscopy ($\Delta R/R$) of the perovskite films as a function of delay times. In our experiment, the wavelength of pump and probe beams is at 785 nm and the convolution of two beams' pulse width is about 290 fs which is determined by an autocorrelator. When measuring, the pump beam was modulated to 4.12 MHz and the probe beam was chopped as 200 Hz. We also set the power of pump and probe as 6 mW and 3 mW, respectively, to avoid heat accumulation effects. The time-dependent $\Delta R/R$ curve exhibits clear multi-exponential decay characteristics, and it can be well-fitted using function $\Delta R/R = A_1\exp(-t/\tau_1) + A_2\exp(-t/\tau_2)$ [28], τ_1 represents the fast decay time constant and τ_2 represents the slow decay time constant, respectively. The decay time constants obtained from the fitting are $\tau_1 = 0.83$ ps (1.5% mass) and $\tau_2 = 53.25$ ps (98.5% mass). Consequently, the average decay lifetime of the $Cs_{0.15}FA_{0.85}PbI_{2.85}Br_{0.15}$ perovskite films SA optical modulators is calculated to be 52.46 ps. This suggests that the $Cs_{0.15}FA_{0.85}PbI_{2.85}Br_{0.15}$ perovskite films SA optical modulators exhibit exceptionally rapid exciton recovery processes within this particular range, suggesting their potential suitability for laser applications [29,30].

Nonlinear optical response of the $Cs_{0.15}FA_{0.85}PbI_{2.85}Br_{0.15}$ perovskite films SA optical modulator were investigated using *Z*-scan. Fig. 4b displays a typical saturable absorption behavior, under the action of excitation pulses with pulse energies of 0.80, 1.64 μJ and 3.21 μJ. The results indicate that the prepared $Cs_{0.15}FA_{0.85}PbI_{2.85}Br_{0.15}$ perovskite films optical modulator exhibits good nonlinear absorption behavior at near-infrared, and the NLO responses of the samples all become stronger with increasing pump pulse energy [31,32]. To further analyze the saturable absorption parameters of $Cs_{0.15}FA_{0.85}PbI_{2.85}Br_{0.15}$ perovskite films SA optical modulator, the experimental data were fitted by the following equation $T(I) = 1\text{-}\alpha_{ns}\exp(-I/I_{sat})-T_{ns}$ [33], where, $T(I)$ represents the transmission of the perovskite film, which refers to the extent to which light passes through the film. α_{ns} represents the modulation depth, which quantifies the relative change in absorption or transmission of the perovskite film as the light intensity varies. I represents the input intensity, indicating the power density of the light beam incident on the perovskite film. I_{sat} represents the saturation intensity, which denotes the threshold intensity at which the absorption or transmission of the perovskite film reaches a saturated state. T_{ns} represents the non-saturable loss, characterizing the level of optical loss in the perovskite film at intensities below the saturation intensity. These parameters are used to describe the optical transmission and modulation characteristics of the perovskite film and are essential for the design and performance evaluation of optical devices. Fig. 5c shows a modulation depth of 15.1% and a saturation intensity of 6.14 MW/cm. The results reveal that the $Cs_{0.15}FA_{0.85}PbI_{2.85}Br_{0.15}$ perovskite films SA optical modulator exhibits variations in nonlinear absorption parameters under different laser parameters, the consistent with the predecessors' research results [34]. Additionally, after each experiment, we placed the samples under an optical microscope for inspection, and no laser-induced damage was observed in any of the perovskite films SA optical modulator. Taking advantage of its high modulation depth, perovskite films can find significant applications in passively Q-switching devices in pulse lasers.

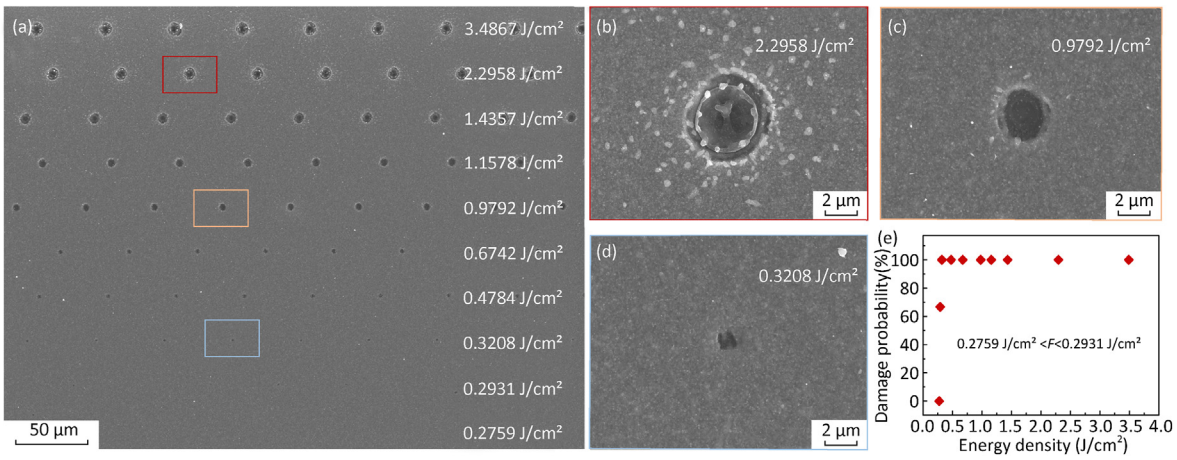

Fig. 3. Damage threshold of the $Cs_{0.15}FA_{0.85}PbI_{2.85}Br_{0.15}$ perovskite films: (a) different energy density; (b) energy density of 2.2958 J/cm^2; (c) energy density of 0.9792 J/cm^2; (d) energy density of 0.3208 J/cm^2; (e) the probability of generating damage points under different energy density.

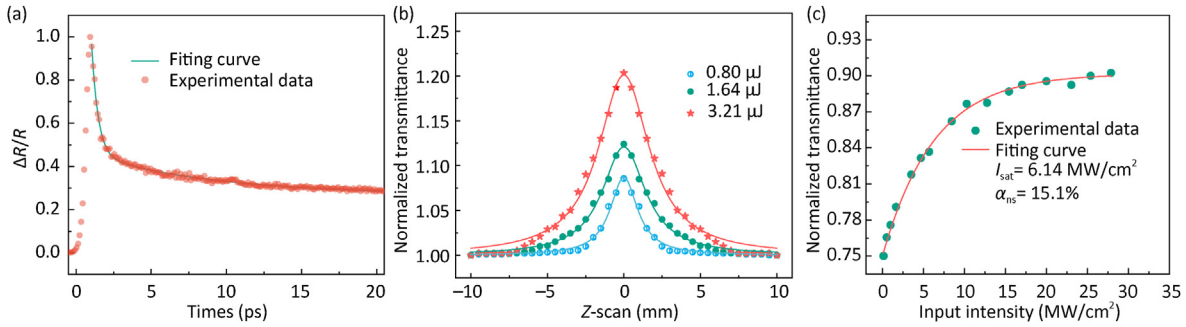

Fig. 4. (a) Time-dependent reflectance changes curves of the $Cs_{0.15}FA_{0.85}PbI_{2.85}Br_{0.15}$ perovskite films SA optical modulators; (b) Nonlinear transmission characteristics of the perovskite films with incident laser energy of 0.80, 1.64 μJ and 3.21 μJ; (c) Relationship between normalized transmittance and input laser intensity with pulse energy of 3.21 μJ.

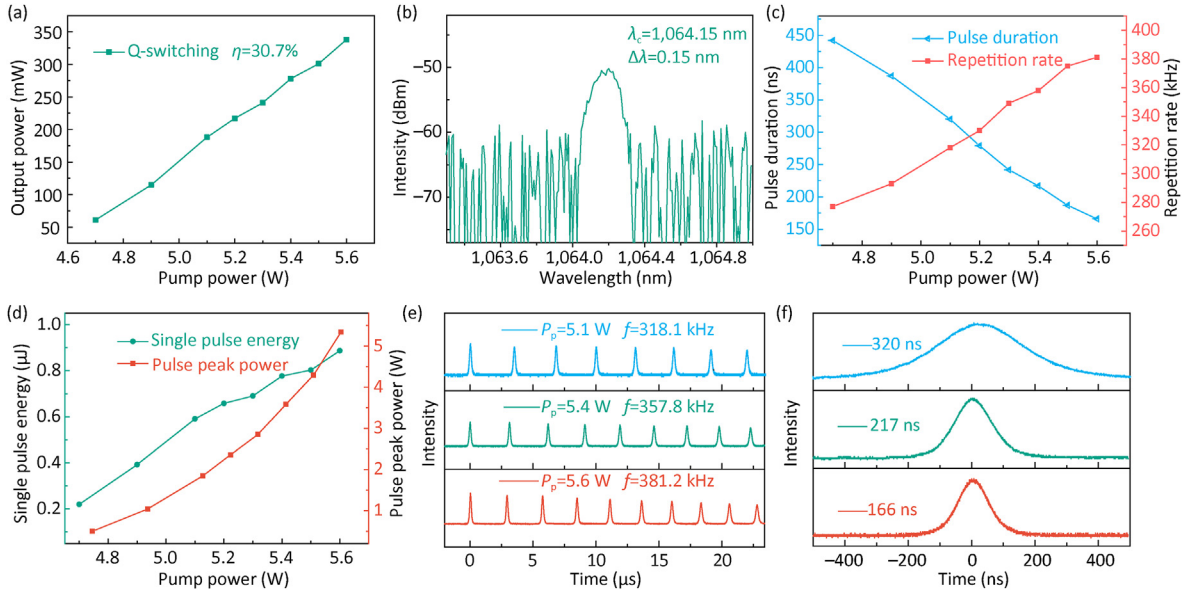

Fig. 5. Passively Q-switched laser: (a) average output power; (b) emission spectrum; (c) repetition rate and pulse duration curves; (d) single pulse energy and peak power curves; (e) pulse trains; and (f) single pulse.

3.4. *Passively Q-switched Nd:YAG laser used $Cs_{0.15}FA_{0.85}PbI_{2.85}Br_{0.15}$ perovskite*

In order to thoroughly investigate the nonlinear optical response characteristics of the $Cs_{0.15}FA_{0.85}PbI_{2.85}Br_{0.15}$ perovskite films SA optical modulator in a laser system. It was inserted into a designed Q-switched Nd:YAG laser oscillator, and adjusting the pump power and the $Cs_{0.15}FA_{0.85}PbI_{2.85}Br_{0.15}$ perovskite SA optical modulator, we achieved short-pulse laser output at 1,064 nm in the near infrared. With the increase of pump power, the average output power of the stable Q-switched laser increases tends to linearly, the slope efficiency reaches 30.7%, and the max-average output power reaches 338 mW, as shown in Fig. 5a. Fig. 5b shows the spectrum of the laser was measured by spectrometer, its central wavelength was 1,064.15 nm. Fig. 5c shows the pulse widths and repetition rates curves under different pump power. When the pump power is up to 5.6 W, the pulse width and repetition rate of laser were 166 ns and 381.2 kHz, respectively, and the corresponding single-pulse energy reached 0.88 μJ, and the peak power was 5.3 W, as depicted in Fig. 5d. When the pump power increases, it leads to a higher energy input into the laser system. This enhanced energy input contributes to an increase in the number of laser pulses generated by stimulated emission, referred to as the pulse repetition rate. Consequently, with a higher pump power, the system can reach the lasing threshold more quickly, resulting in a reduced pulse duration. This relationship between pump power and pulse characteristics is illustrated in Fig. 5e. When pump power is 5.1, 5.4, 5.6 W, the output pulse frequency is 318.1, 357.8, 381.2 kHz, respectively. The corresponding pulse width are 320, 217 ns and 166 ns respectively, as shown in Fig. 5f.

In Table 1, the performance characteristics of passively solid-state Q-switched at 1,064 nm lasers employing various perovskite materials as SA optical modulator were summarized. Compared to other perovskite materials, the stable output power of the 1,064 nm solid-state Q-switched laser achieved by the $Cs_{0.15}FA_{0.85}Pb_{12.85}Br_{0.15}$ perovskite films is higher and the pulse width is shorter, which has an excellent commercial value. It is worth noting that low-dimensional perovskite can still exhibit saturation absorption response even when the bandgap is larger than the energy of the excitation light. This is attributed to the saturation of free-carrier absorption by subgap trap states [13].

3.5. *Stability of perovskite films SA optical modulators*

To investigate the thermal stability of the $Cs_{0.15}FA_{0.85}Pb_{I2.85}Br_{0.15}$ perovskite SA optical modulator, we conducted a comparative

Table 1
Comparison of Q-switched lasers with different perovskite SA.

SA type	Laser type	Wavelength (nm)	Pulse duration (ns)	Average output power (mW)	Ref.
$CH_3NH_3PbI_3$	Nd:YGG	1,064	305	29	[3]
$CH_3NH_3PbI_3$	Nd:YVO_4	1,064	181.6	182	[35]
$CsPbBr_3$	Nd:YVO_4	1,064	69	240	[36]
$CH_3NH_3PbBr_3$	Nd:YVO_4	1,064	686	115	[37]
$Cs_{0.15}FA_{0.85}PbI_{2.85}Br_{0.15}$	Nd:YAG	1,064	166	338	**Our work**

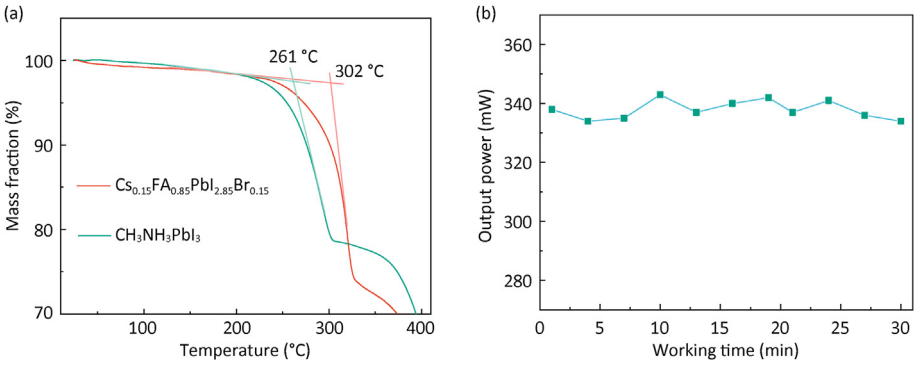

Fig. 6. (a) TG curves for $Cs_{0.15}FA_{0.85}PbI_{2.85}Br_{0.15}$ and $CH_3NH_3PbI_3$ perovskite; (b) Continuous operation stability of the $Cs_{0.15}FA_{0.85}PbI_{2.85}Br_{0.15}$ perovskite SA.

analysis by the thermal gravimetric analysis. The results are illustrated in Fig. 6a—and a notable distinction observed in the high-temperature thermal decomposition test between $Cs_{0.15}FA_{0.85}PbI_{2.85}Br_{0.15}$ and the commonly reported $CH_3NH_3PbI_3$ were the temperature threshold for gas release. Specifically, the $Cs_{0.15}FA_{0.85}PbI_{2.85}Br_{0.15}$ perovskite exhibited a temperature threshold of 302 °C, while the $CH_3NH_3PbI_3$ perovskite had a threshold of 261 °C. This indicates a higher decomposition temperature for the $Cs_{0.15}FA_{0.85}PbI_{2.85}Br_{0.15}$ perovskite compared to the $CH_3NH_3PbI_3$ perovskite, which is consistent with previous research [38,39]. Furthermore, we assessed its stability over prolonged continuous operation under laser illumination, as illustrated in Fig. 6b. After half an hour of continuous operation, the output power exhibited minimal decline, strongly indicating excellent stability in modulation capability for this perovskite SA. These findings underscore the well-preserved performance stability of the perovskite thin films, which holds significant promise for the fabrication of potential nonlinear photonic devices.

4. Conclusions

In summary, we have reported an efficient SA optical modulator with the thermally stable $Cs_{0.15}FA_{0.85}PbI_{2.85}Br_{0.15}$ perovskite towards solid-state Q-switched lasers for the first time. A perovskite films of superior quality was created and its nonlinear optical characteristics were detailed investigated. The saturable intensity, modulation depth and recovery time of $Cs_{0.15}FA_{0.85}PbI_{2.85}Br_{0.15}$ perovskite films SA optical modulator were measured to be 6.14 MW/cm^2, 15.1% and 52.46 ps, respectively. Additionally, the perovskite films' damage threshold was estimated to exceed 275.9 mJ/cm^2. The developed perovskite films functioned as a SA optical modulator enabling the successful fabrication of a laser with a center wavelength of 1,064.15 nm. The output power reached a maximum average of 338 mW at a repetition frequency of 381.2 kHz, while the minimum pulse duration is 166 ns. This work demonstrates the unique nonlinear properties of the $Cs_{0.15}FA_{0.85}PbI_{2.85}Br_{0.15}$ perovskite material and its potential applications in near-infrared.

Declaration of competing interest

The authors declare that they have no known competing financial interests or personal relationships that could have appeared to influence the work reported in this paper.

Acknowledgments

This project was financially supported by the National Natural Science Foundation of China (62205187, 62127817, U22A2091, and 62222509), the Fundamental Research Program of Shanxi Province (202103021223032), Key Industrial Chain Core Technology Research Projects of Xi'an (23ZDCYJSGG0041-2022), and the interdisciplinary construction project of Shanxi University. In addition, the authors thank Hong Chang at the Institute of Earth Environment and ChangAn Frontier Aerospace Intelligent Manufacturing Laboratory for them for their kind help in theresearch work.

References

[1] Kumar NS, Naidu KC. A review on perovskite solar cells (PSCs), materials and applications. J Materiomics 2021;7(5):940–56.
[2] Yang ZC, Zhang SS, Li LB, Chen W. Research progress on large-area perovskite thin films and solar modules. J Materiomics 2017;3(4):231–44.
[3] Zhang R, Fan JD, Zhang X, Yu HH, Zhang HJ, Mai YH, et al. Nonlinear optical response of organic-inorganic halide perovskites. ACS Photonics 2016;3:371–7.
[4] Ding K, Ye HS, Su CY, Xiong YA, Du GW, You YM, et al. Superior ferroelectricity and nonlinear optical response in a hybrid germanium iodide hexagonal perovskite. Nat Commun 2023;14(1):2863.
[5] Wang G, Liu TH, Wang BZ, Gu H, Wei Q, Zhang ZP, et al. Hot-carrier tunable abnormal nonlinear absorption conversion in quasi-2D perovskite. Nat Commun 2022;13(1):6935.
[6] Guan ZH, Fu LL, Wei ZY, Shan NY, Li H, Fang Y, et al. Toward strong nonlinear optical absorption properties of perovskite films *via* porphyrin axial passivation. Mater Today Phys 2023;35:101135.
[7] Zhang HJ, Song T, Liu XX, Chen MZ, Ma B, Huang HZ, et al. Lead-free double-perovskite $Cs_4CuSb_2Cl_{12}$ as an efficient saturable absorber for Q-switched mode-locking fiber. J Mater Chem C 2023;11:14127–33.
[8] Yang S, Li JZ, Li L, Zhang L, Zhang XW. Mode-locking operation of an Er-doped fiber laser with $(PEA)_2(CsPbBr_3)_{n-1}PbBr_4$ perovskite saturable absorbers. J Mater Chem C 2022;10(19):7504–10.
[9] Guo PL, An MQ, Shu YQ, Peng XL, Han YH, Hu HG, et al. Nonlinear photonics

device based on double perovskite oxide Ba_2LaTaO_6 for ultrafast laser generation. Opt Laser Technol 2022;155:108334.
[10] Guan ZH, Li H, Wei ZY, Shan NY, Fang Y, Zhao Y, et al. Enhanced nonlinear optical performance of perovskite films passivated by porphyrin derivatives. J Mater Chem C 2023;11(4):1509–21.
[11] Han X, Zheng YS, Chai SQ, Chen SH, Xu JL. 2D organic-inorganic hybrid perovskite materials for nonlinear optics. Nanophotonics 2020;9(7):1787–810.
[12] Zhou YX, Huang YY, Xu XL, Fan ZY, Khurgin JB, Xiong QH. Nonlinear optical properties of halide perovskites and their applications. Appl Phys Rev 2020;7(4):041313.
[13] Chen WQ, Zhang F, Wang C, Jia MS, Zhao XH, Liu ZR, et al. Nonlinear photonics using low-dimensional metal-halide perovskites: recent advances and future challenges. Adv Mater 2021;33(11):2004446.
[14] Zhao XL, Jin H, Liu JY, Chao JL, Liu TY, Zhang H, et al. Integration and applications of nanomaterials for ultrafast photonics. Laser Photon Rev 2022;16(11):2200386.
[15] Shang XX, Zhang YL, Li T, Zhang HN, Zou XF, Wageh S, et al. Nonlinear optical response of niobium telluride and its application for demonstrating pulsed fiber lasers. J Materiomics 2023;52:8478.
[16] Dong L, Chu HW, Li Y, Zhao SZ, Li D. Third-order nonlinear optical responses of CuO nanosheets for ultrafast pulse generation. J Materiomics 2022;8(2):511–7.
[17] Wang J, Li GY, Liu SC, Chai JS, Wang YG, Cheng GH. Nonlinear absorption response of zirconium carbide films. ACS Appl Mater Interfaces 2023;15:3317–24.
[18] Fu WF, Ricciardulli AG, Akkerman Q, John RA, Tavakoli MM, Essig S, et al. Stability of perovskite materials and devices. Mater Today 2022;58:275–96.
[19] Yan J, Zhao JS, Wang HX, Kerklaan M, Bannenberg LS, Ibrahim B, et al. Crystallization process for high-quality $Cs_{0.15}FA_{0.85}PbI_{2.85}Br_{0.15}$ films deposited via simplified sequential vacuum evaporation. ACS Appl Energy Mater 2023;6(20):10265–73.
[20] Dörflinger P, Ding Y, Schmid V, Armer M, Turnell R, Ding B, et al. Influence of an organic salt-based stabilizing additive on charge carrier dynamics in triple cation perovskite solar cells. Adv Sci 2023;10(34):2304502.
[21] Eperon GE, Stranks SD, Menelaou C, Johnston MB, Herz LM, Snaith HJ. Photovoltaic mixed-cation lead mixed-halide perovskites: links between crystallinity, photo-stability and electronic properties. Energy Environ Sci 2014;7:982.
[22] Wang SX, Pang SZ, Chen DZ, Zhu WD, Xi H, Zhang CF. Improving perovskite solar cell performance by compositional engineering *via* triple-mixed cations. Sol Energy 2021;220:412–7.
[23] Yan J, Stickel LS, Hengel L, Wang HX, Anusuyadevi PR, Kooijman A, et al. Vacuum deposited perovskites with a controllable crystal orientation. J Phys Chem Lett 2023;14(39):8787–95.
[24] Zhu HW, Teale S, Lintangpradipto MN, Mahesh S, Chen B, McGehee M, et al. Long-term operating stability in perovskite photovoltaics. Nat Rev Mater 2023;8(9):569–86.
[25] Xing XW, Liu YX, Han JF, Liu WJ, Wei ZY. Preparation of high damage threshold device based on Bi_2Se_3 films and its application in fiber lasers. ACS Photonics 2023;10(7):2264–71.
[26] Liu XC, Zeng P, Chen SH, Smith TA, Liu MZ. Charge transfer dynamics at the interface of $CsPbX_3$ perovskite nanocrystal-acceptor complexes: a femtosecond transient absorption spectroscopy study. Laser Photon Rev 2022;16(12):2200280.
[27] Zhang JJ, Zhu BC, Zhang LY, Yu JG. Femtosecond transient absorption spectroscopy investigation into the electron transfer mechanism in photocatalysis. Chem Commun 2023;59(6):688–99.
[28] Lee K, Kwon SY, Woo T, Ryu J, Jung J, Lee JH. Nonlinear absorption and refraction properties of V_4C_3 MXene and its use for an ultra-broadband saturable absorber. Adv Opt Mater 2023;11(13):2300213.
[29] Rafique MZ, Basiri A, Bai J, Zuo JW, Yao Y. Ultrafast graphene-plasmonic hybrid metasurface saturable absorber with low saturation fluence. ACS Nano 2023;17(11):10431–41.
[30] Mihnev MT, Kadi F, Divin CJ, Winzer T, Lee S, Liu CH, et al. Microscopic origins of the terahertz carrier relaxation and cooling dynamics in graphene. Nat Commun 2016;7(1):11617.
[31] Zhang L, Liu J, Li J, Wang Z, Wang Y, Ge Y, et al. Site-selective Bi_2Te_3–$FeTe_2$ heterostructure as a broadband saturable absorber for ultrafast photonics. Laser Photon Rev 2020;14(4):1900409.
[32] Gao LF, Chen HL, Kuklin AV, Wageh S, Al-Ghamdi AA, Agren H, et al. Optical properties of few-layer Ti_3CN MXene: from experimental observations to theoretical calculations. ACS Nano 2022;16(2):3059–69.
[33] Liu WJ, Zhu YN, Liu ML, Wen B, Fang SB, Teng H, et al. Optical properties and applications for MoS_2-Sb_2Te_3-MoS_2 heterostructure materials. Photon Res 2018;6(3):220–7.
[34] Xu JL, Li XY, Xiong JB, Yuan CQ, Semin S, Rasing T, et al. Halide perovskites for nonlinear optics. Adv Mater 2020;32(3):1806736.
[35] Wang J, Wang YG, Wang TJ, Liu SC, Wang H, Dong T, et al. 1.34μm Q-switched Nd:YVO_4 laser based on perovskite films saturable absorber. IEEE Photon Technol Lett 2019;32(1):3–6.
[36] Zhang XL, Zhang YW, Xu RQ, Pan JB, Hu L, Duan WJ, et al. 2D self-assembled perovskite nanosheets as a nonlinear saturable absorber for passive Q-switched laser. J Lumin 2023;253:119453.
[37] Dong SY, Zhang C, Zhou YX, Miao XN, Zong TT, Gu MN, et al. High-stability hybrid organic-inorganic perovskite ($CH_3NH_3PbBr_3$) in SiO_2 mesopores: nonlinear optics and applications for Q-switching laser operation. Nanomaterials 2021;11(7):1648.
[38] Ma L, Guo DQ, Li MT, Wang C, Zhou ZL, Zhao X, et al. Temperature-dependent thermal decomposition pathway of organic–inorganic halide perovskite materials. Chem Mater 2019;31(20):8515–22.
[39] Juarez-Perez EJ, Ono LK, Qi YB. Thermal degradation of formamidinium based lead halide perovskites into sym-triazine and hydrogen cyanide observed by coupled thermogravimetry-mass spectrometry analysis. J Mater Chem A 2019;7(28):16912–9.

Jiang Wang is a Associate Professor and the School of Artificial intelligence, Optics and Electronics (iOPEN), Northwestern Polytechnical University. He obtained his Ph.D. degrees at Shaanxi Normal Universityin China in July 2020. His current research focus is the ultrafast and nonlinear photonics of materials, *i.e.*, MXenes and perovskite.

Zhichun Yang received his Ph.D. degree from Huazhong University of Science and Technology (China) in 2021. He is currently an associate professor at the State Key Laboratory of Quantum Optics and Quantum Optics Devices, Shanxi University, China. His research mainly focuses on semiconductor optoelectronic devices, including perovskite solar cells, light emitting diode, photodetectors and imagers.

Prof. Guanghua Cheng received his Ph.D. degree from in Xi'an Institute of Optics and Precision Mechanics of CAS. He obtained his B.S. degree at Physics Department, Northwest University in China. Now he is a full-professor at the Northwestern Polytechnical University. His current research interests include ultrafast laser machining and processes, high power solid laser technique and interaction between ultrafast laser and mater, nonlinear optics.